Inorg. Chem. **2008**, *47*, 1965−1974

Disorder and Intermolecular Interactions in a Family of Tetranuclear Ni(II) Complexes Probed by High-Frequency Electron Paramagnetic Resonance

Jon Lawrence,[†] En-Che Yang,[‡] Rachel Edwards,[†] Marilyn M. Olmstead,[§] Chris Ramsey,[⊥] Naresh S. Dalal,[⊥] Peter K. Gantzel,[‡] Stephen Hill,*[,†] and David N. Hendrickson*[,‡]

Department of Physics, University of Florida, Gainesville, Florida 32611-8440, Department of Chemistry and Biochemistry, University of California at San Diego, La Jolla, California 92093-0358, Department of Chemistry and National High Magnetic Field Laboratory, Florida State University, Tallahassee, Florida 32306, and Department of Chemistry, University of California at Davis, Davis, California 95616

Received July 16, 2007

High-frequency electron paramagnetic resonance (HFEPR) data are presented for four closely related tetranuclear Ni(II) complexes, $[Ni(hmp)(MeOH)Cl]_4 \cdot H_2O$ (**1a**), $[Ni(hmp)(MeOH)Br]_4 \cdot H_2O$ (**1b**), $[Ni(hmp)(EtOH)Cl]_4 \cdot H_2O$ (**2**), and $[Ni(hmp)(dmb)Cl]_4$ (**3**) (where hmp^- is the anion of 2-hydroxymethylpyridine and dmb is 3,3′-dimethyl-1-butanol), which exhibit magnetic bistability (hysteresis) and fast magnetization tunneling at low temperatures, properties which suggest they are single-molecule magnets (SMMs). The HFEPR spectra confirm spin $S = 4$ ground states and dominant uniaxial anisotropy ($D\hat{S}_z^2$, $D < 0$) for all four complexes, which are the essential ingredients for a SMM. The individual fine structure peaks (due to zero-field splitting) for complexes **1a**, **1b**, and **2** are rather broad. They also exhibit further (significant) splitting, which can be explained by the fact that there exists two crystallographically distinct Ni_4 sites in the lattices for these complexes, with associated differences in metal–ligand bond lengths and different zero-field splitting (ZFS) parameters. The broad EPR lines, meanwhile, may be attributed to ligand and solvent disorder, which results in additional distributions of microenvironments. In the case of complex **3**, there are no solvate molecules in the structure, and only one distinct Ni_4 molecule in the lattice. Consequently, the HFEPR data for complex **3** are extremely sharp. As the temperature of a crystal of complex **3** is decreased, the HFEPR spectrum splits abruptly at ∼46 K into two patterns with very slightly different ZFS parameters. Heat capacity data suggest that this is caused by a structural transition at 46.6 K. A single-crystal X-ray structure at 12(2) K indicates large thermal parameters on the terminal methyl groups of the dmb (3,3-dimethyl-1-butanol) ligand. Most likely there exists dynamic disorder of parts of the dmb ligand above 46.6 K; an order–disorder structural phase transition at 46.6 K then removes some of the motion. A further decrease in temperature (<6 K) leads to further fine structure splittings for complex **3**. This behavior is thought to be due to the onset of short-range magnetic correlations/coherences between molecules caused by weak intermolecular magnetic exchange interactions.

Introduction

Single-molecule magnets (SMMs), discovered in 1993,[1,2] are molecular nanomagnets that have a barrier for magnetization reversal due to a relatively large spin (S) ground-state experiencing negative magnetoanisotropy, $D\hat{S}_z^2$ (with $D < 0$).[3–5] The ability to synthesize polynuclear, monodisperse, noninteracting magnetic nanoparticles provides an arena for important studies of quantum mechanical processes involving spins, e.g., quantum tunneling of magnetization

* To whom correspondence should be addressed. E-mail: dhendrickson@ucsd.edu (D.N.H.), hill@phys.ufl.edu (S.H.).
[†] University of Florida.
[‡] University of California at San Diego.
[§] University of California at Davis.
[⊥] Florida State University.

(1) Sessoli, R.; Tsai, H. L.; Schake, A. R.; Wang, S. Y.; Vincent, J. B.; Folting, K.; Gatteschi, D.; Christou, G.; Hendrickson, D. N. *J. Am. Chem. Soc.* **1993**, *115*, 1804–1816.

10.1021/ic701416w CCC: $40.75
Published on Web 02/20/2008

(QTM).[6,7] One important area of active research involves investigations of how the magnetic behavior of a magnetic molecule is influenced by its surrounding environment.[8–13]

In this paper, we employ high-frequency electron paramagnetic resonance (HFEPR) spectroscopy to study single-crystals of four related tetranuclear Ni(II) complexes having the composition $[Ni(hmp)(ROH)X]_4$, where hmp^- is the anion of 2-hydroxymethylpyridine, R is an alkyl substituent [either CH_3, CH_2CH_3, or $CH_2CH_2C(CH_3)_3$] and X^- is either Cl^- or Br^-. In each instance, the anisotropic Ni(II) ions couple ferromagnetically giving rise to a spin $S = 4$ ground state with a dominant uniaxial anisotropy, as required for a SMM. However, very recently, we reported extremely fast QTM in this series of complexes.[14] The HFEPR data allow us to characterize the zero-field splitting (ZFS) parameters as well as the disorder associated with these interesting molecular nanomagnets. The data reveal multiple species within a crystal due to differing microenvironments, which manifest themselves as multiple ground-state transitions (i.e., splittings of the EPR transition peaks), as well as broad and unusually shaped EPR peaks resulting from disorder-induced *D*-strain (m_s-dependent linewidths). Additionally, intermolecular exchange interactions, while present in all complexes, are most clearly resolved in the complex having the sharpest linewidths [$R = CH_2CH_2C(CH_3)_3$, $X^- = Cl^-$]. The effects of exchange can be inferred from additional splittings of the ground-state transition peak at low temperatures that cannot be explained in terms of either a structural transition or to *D*-strain. The sharp EPR spectra found for this one complex appear to be due to the fact that the structure contains no solvate molecules. Thus, these investigations further highlight[10] the significant influence of weakly interacting solvate molecules on the quantum properties of SMMs.

Experimental Section

All of the compounds $[Ni(hmp)(MeOH)Cl]_4 \cdot H_2O$ (**1a**), $[Ni(hmp)(MeOH)Br]_4 \cdot H_2O$ (**1b**), $[Ni(hmp)(EtOH)Cl]_4 \cdot H_2O$ (**2**), and $[Ni(hmp)(dmb)Cl]_4$ (**3**) (where dmb is 3,3′-dimethyl-1-butanol) were prepared as previously reported;[14] detailed structural information for all of these and related complexes can also be found in ref 14. The morphology of a typical single crystal is square pyramidal with a volume on the order of one to several cubic millimeters. For this sample morphology, the crystal *c*-axis is directed along the apex of the pyramid, with the faces defined by (101), (011), etc. To the best of our knowledge, all molecules are oriented such that their magnetic easy axes are parallel to the crystallographic *c*-axis.

Single-crystal HFEPR data were collected using a millimeter-wave vector network analyzer (MVNA) and a high-sensitivity cavity perturbation technique described elsewhere.[15,16] Experiments on complexes **1a**, **1b**, and **2** were performed in a commercial 7 T horizontal field (split-pair) superconducting magnet associated with a Quantum Design Physical Properties Measurement System (QD PPMS). Single-crystal samples were mounted on the end plate of a cylindrical (TE01*n*, n = integer) copper cavity with a small amount of silicone grease. Orientation of the sample with respect to the magnetic field was achieved in two ways: by rotation of the entire waveguide and cavity assembly within the bore of the split-pair magnet using a computer controlled stepper motor, providing angle resolution of 0.01°; and in situ rotation of the end plate of the cavity using a manual externally driven worm gear (a resolution of 0.18°).[16] These two methods allow for full rotation of the sample about orthogonal axes. Experiments on complex **3** were performed in an Oxford Instruments 17 T vertical field superconducting magnet using a fixed vertical cylindrical TE01*n* cavity. The very regular shape of crystals of complex **3** enabled precise orientation of the sample within the cavity such that the field was aligned with its *c*-axis. For all HFEPR measurements, the temperature was regulated using He flow cryostats and Cernox resistance sensors for thermometry.

Specific heat at constant pressure (C_P) versus temperature measurements were made at zero-field using a Quantum Design PPMS employing a relaxation method.[17] The specific heat sensor was calibrated by means of a copper standard.

X-ray Structure Determination of $[Ni(hmp)(dmb)Cl]_4$ (3). A single green block crystal of dimensions 0.26 × 0.24 × 0.14 mm was mounted in the 12(2) K helium cold stream provided by a CRYO Industries CRYOCOOL-LHE apparatus on the goniometer head of a Bruker SMART Apex II diffractometer. A total of 20067 reflections were collected with graphite-monochromated Mo Kα radiation to $2\theta_{max}$ of 55°. A multiscan correction for absorption was applied using the program SADABS 2.10. The unique set of data has 3294 reflections (R(int) = 0.060) and 2855 were observed ($I > 2\sigma(I)$). The structure was solved by direct methods (SHELXS97) and refined by full-matrix least-squares on F^2 (SHELXL97). The maximum and minimum peaks in the final difference Fourier map corresponded to 0.635 and −0.533 eÅ^{-3}. Crystal data: $C_{48}H_{80}Cl_4N_4Ni_4O_8$, M = 1217.80, tetragonal, space group $I4_1/a$, a = 12.8052(12) Å, c = 34.940(7) Å, Z = 4. The refinement converged with a wR2 value of 0.0707 using all data and an R1 value of 0.0331 for observed data using 161 parameters. Data collection, Apex2; data reduction, SAINT version 7.06; Bruker Analytical X-ray Instruments, Inc., Madison, WI, 2004. SADABS 2.10. Sheldrick, G.M., 2003. University of Göttingen, Germany. SHELXS97 and SHELXL97. Sheldrick, G.M. SHELXTL v. 5.10; Bruker Analytical X-ray Instruments, Inc., Madison, WI, 1997.

(2) Sessoli, R.; Gatteschi, D.; Caneschi, A.; Novak, M. A. *Nature* **1993**, *365*, 141–143.
(3) Christou, G.; Gatteschi, D.; Hendrickson, D. N.; Sessoli, R. *MRS Bull.* **2000**, *25*, 66.
(4) Gatteschi, D.; Sessoli, R. *Angew. Chem.* **2003**, *42*, 268.
(5) Gatteschi, D.; Sessoli, R.; Villain, J. *Molecular Nanomagnets*; Oxford University Press: Oxford, U.K., 2006.
(6) Friedman, J. R.; Sarachik, M. P.; Tejada, J.; Ziolo, R. *Phys. Rev. Lett.* **1996**, *76*, 3830.
(7) Thomas, L.; Lionti, F.; Ballou, R.; Sessoli, R.; Gatteschi, D.; Barbara, B. *Nature* **1996**, *383*, 145.
(8) Cornia, A.; Sessoli, R.; Sorace, L.; Gatteschi, D.; Barra, A. L.; Daiguebonne, C. *Phys. Rev. Lett.* **2002**, *89*, 257201.
(9) Chudnovsky, E. M.; Garanin, D. A. *Phys. Rev. Lett.* **2001**, *87*, 187203.
(10) Hill, S.; Edwards, R. S.; Jones, S. I.; Dalal, N. S.; North, J. M. *Phys. Rev. Lett.* **2003**, *90*, 217204.
(11) del Barco, E.; Kent, A. D.; Rumberger, E. M.; Hendrickson, D. N.; Christou, G. *Phys. Rev. Lett.* **2003**, *91*, 047203.
(12) Park, K.; Baruah, T.; Bernstein, N.; Pederson, M. R. *Phys. Rev. B* **2004**, *69*, 144426.
(13) del Barco, E.; Kent, A. D.; Hill, S.; North, J. M.; Dalal, N. S.; Rumberger, E. M.; Hendrickson, D. N.; Chakov, N.; Christou, G. *J. Low Temp. Phys.* **2005**, *140*, 119–174.
(14) Yang, E.-C.; Wernsdorfer, W.; Zakharov, L.; Karaki, Y.; Yamaguchi, A.; Isidro, R.; Lu, G. D.; Wilson, S.; Rheingold, A.; Ishimoto, H.; Hendrickson, D. N. *Inorg. Chem.* **2006**, *45*, 529–546.
(15) Mola, M.; Hill, S.; Goy, P.; Gross, M. *Rev. Sci. Instrum.* **2000**, *71*, 186–200.
(16) Takahashi, S.; Hill, S. *Rev. Sci. Instrum.* **2005**, *76*, 023114.
(17) Schmiedeshoff, G. M.; Fortune, N. A.; Brooks, J. S.; Stewart, G. R. *Rev. Sci. Instrum.* **1987**, *58*, 1743–1745.

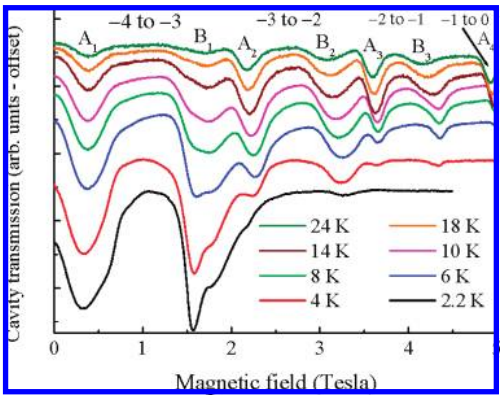

Figure 1. Single-crystal HFEPR spectra for complex **1a** taken at 175 GHz with the magnetic field approximately aligned with the crystal *c*-axis. The A resonances correspond to one molecular species, and the B resonances to the other.

Results and Discussion

HFEPR Data for the MeOH and EtOH Complexes. Figure 1 displays single-crystal HFEPR spectra for the MeOH complex **1a** taken at 175 GHz in the range from 0 to 5 T and at temperatures between 2.2 and 24 K. The sample was oriented so that the magnetic field is approximately aligned with the crystal *c*-axis; this was deduced on the basis of angle-dependent HFEPR measurements (not shown).[18] The dips in the transmission through the cavity correspond to EPR absorption. Attention is first drawn to the 10 K spectrum: it can be seen that there are seven major peaks labeled A_1 to A_4 and B_1 to B_3. We shall discuss the unusual EPR lineshapes at the end of this section. As the temperature is increased to 24 K, the intensities of the low field peaks (0 to 3 T) decrease dramatically, whereas the relative intensities of the higher field peaks (3 to 5 T) increase. On the other hand, when the temperature is decreased from 10 K, the higher field peaks disappear, whereas the two broad peaks below 2 T (A_1 and B_1) become very strong. These changes in relative intensities with changes in temperature reveal that the A_1 and B_1 peaks correspond to transitions from the ground state ($m_S = -4$ to -3), and that the peaks at higher resonance fields result from transitions between higher energy states (e.g., $m_S = -3$ to -2 and $m_S = -2$ to -1, as labeled in the figure). Upon closer inspection, one finds from the temperature dependence of the peaks that they can be grouped into pairs: A_1 and B_1, A_2 and B_2, A_3 and B_3, etc. This fact implies that there are two distinct Ni_4 molecular species in the crystal lattice, with different ZFS parameters. Thus, the A resonances correspond to one molecular species, and the B resonances to the other, hence the two ground-state transitions. This result agrees with the X-ray crystallography for complexes **1a**, **1b**, and **2**, where it is found that there are two crystallographically independent molecules in the lattice, one at the body center and the other at the *C*-face center.[14]

To determine the ZFS parameters for the A and B molecules, the temperature was held constant and spectra were taken at different frequencies. Panels a and b in Figure 2, respectively, plot the positions of the A and B resonances for complex **1a** as a function of the measurement frequency. The data have been fit to the following effective spin Hamiltonian eq 1 to give the straight lines shown in the figure

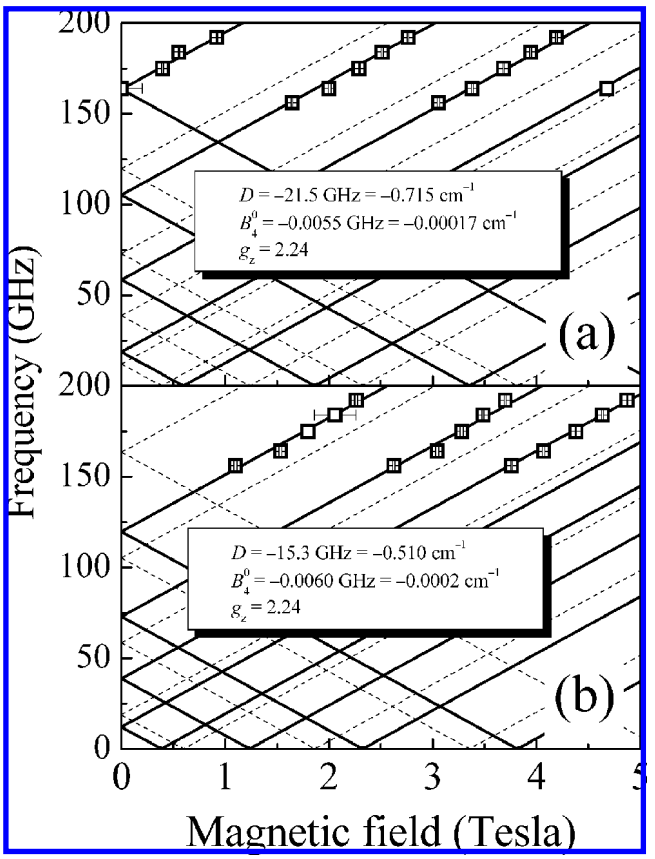

Figure 2. Plots of the positions of the A and B resonances for complex **1a** obtained at 10 K, as a function of the measurement frequency. The data have been fit to eq 1 with an $S = 4$ ground state.

$$\hat{H} = g_z \mu_B B_z \hat{S}_z + D\hat{S}_z^2 + B_4^0 \hat{O}_4^0 \quad (1)$$

Here, $\hat{S}_z$ is the *z*-component spin operator, B_z is the magnetic field component along the *c*-axis of the crystal, g_z is the *z*-component of the Landé g-tensor, μ_B is the Bohr magneton, and the final term represents the fourth-order axial ZFS interaction.[3] We note that the fourth-order parameter is rather artificial in this giant-spin parametrization, because fourth-order anisotropy is forbidden for spin $s = 1$ Ni^{II}. However, in a separate publication,[19] we have clearly demonstrated that the origin of fourth-order terms (both axial and transverse) is related to admixing of higher-lying spin multiplets (with $S < 4$) to the ground-state multiplet via the competing isotropic (exchange) and anisotropic (spin–orbit) interactions in a spin Hamiltonian expressed in the basis of the four uncoupled Ni^{II} ions, i.e., this is due to a breakdown of the strong exchange approximation. Nevertheless, for the purposes of the present study, one can gain sufficient insight on the basis of the far simpler giant-spin parametrization including effective fourth order terms, i.e. one gains nothing extra from an analysis starting from the uncoupled Ni^{II} ion

(18) Stamatatos, T. C.; Foguet-Albiol, D.; Stoumpos, C. C.; Lee, S.-C.; Hill, S. O.; Raptopoulou, C. P.; Terzis, A.; Wernsdorfer, W.; Perlepes, S. P.; Christou, G. *J. Am. Chem. Soc.* **2007**, *129*, 9484.

(19) Wilson, A.; Lawrence, J.; Yang, E.-C.; Nakano, M.; Hendrickson, D. N.; Hill, S. *Phys. Rev. B* **2006**, *74*, R140403.

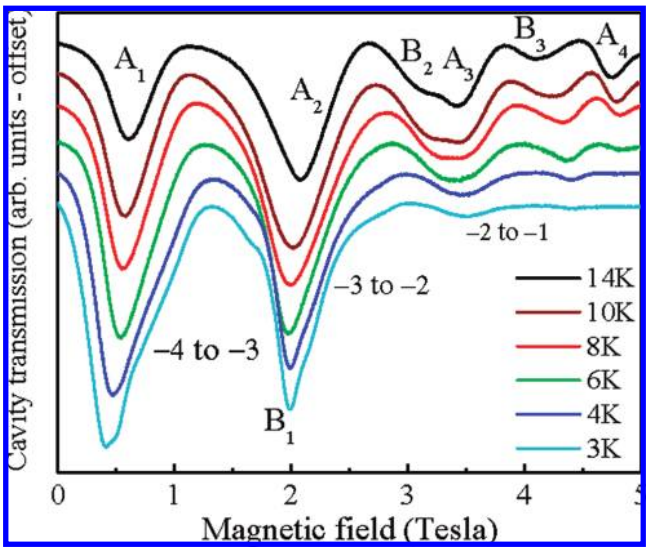

Figure 3. Easy axis HFEPR data for a single crystal of complex **1b** at 163 GHz. As with complex **1a**, the A resonances correspond to one molecular species, and the B resonances to the other.

basis. As can be seen, both sets of peaks (A and B) independently give a good fit to eq 1, with different sets of ZFS parameters (given in the figure). It should be noted that easy axis measurements ($B//c$) only provide information concerning the diagonal terms in the spin Hamiltonian (interactions which commute with the Zeeman and dominant $D\hat{S}_z^2$ terms). For this reason, we have omitted the transverse terms in eq 1, which represent the focus of a separate investigation.[19]

The fits in Figure 2 further support the assignment of the two sets of EPR peaks to the two crystallographically distinct Ni_4 SMMs in the crystal of complex **1**. Note also that both species have $S = 4$ ground states. The subscripts 1, 2, 3, and 4 in the two series correspond respectively to the following fine structure transitions: $m_S = -4$ to -3, $m_S = -3$ to -2, $m_S = -2$ to -1 and $m_S = -1$ to 0. The obtained axial ZFS parameters are: $g_z = 2.24(5)$, $D = -0.715(7)$ cm^{-1}, $B_4^0 = -0.00017(4)$ cm^{-1} for species A, and $g_z = 2.24(5)$, $D = -0.510(6)$ cm^{-1}, $B_4^0 = -0.00020(4)$ cm^{-1} for species B. Assuming that the two series of resonances arise from the distinct species occupying the body center and *C*-face center of the unit cell,[14] then the corresponding A_i and B_i EPR resonances should have similar intensities, because these two species occur in equal populations. Indeed, this does appear to be the case, yielding an average value for the axial ZFS parameter of $D = -0.60$ cm^{-1}, which is in excellent agreement with the value obtained from reduced magnetization measurements, which give a value of $D = -0.61$ cm^{-1} for a powder sample.[14]

Very similar HFEPR data were obtained for a single crystal of complex **1b**, $[Ni(hmp)(MeOH)Br]_4$. Easy axis spectra obtained at 163 GHz are displayed in Figure 3. As with complex **1a**, two series of resonances are seen, which are again labeled A and B. The splitting of the A_1 and B_1 ground-state peaks is a little larger for complex **1b** resulting in an overlap of the A_2 and B_1 peaks. Thus, the grouping of resonances into pairs is not quite as obvious as it is in Figure 1. However, it is very clear from the lowest temperature

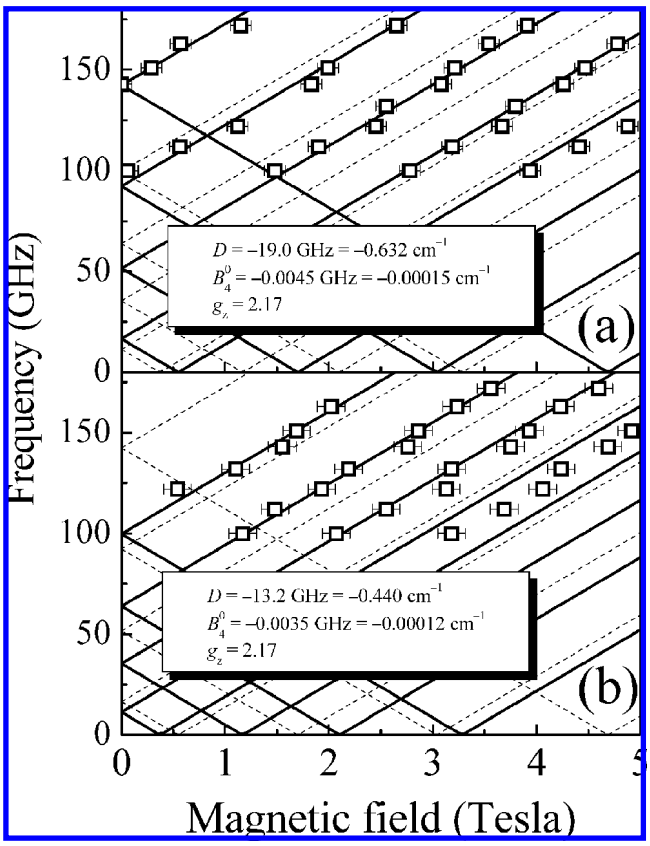

Figure 4. Plots of the positions of the A and B resonances for complex **1b** obtained at 10 K, as a function of the measurement frequency. The data have been fit to eq 1 with an $S = 4$ ground state. The qualitative trends in the data and the obtained ZFS parameters for complex **1a** and **1b** are very similar.

spectrum that the sample contains two dominant species, giving rise to the A_1 and B_1 resonances. Because of the overlapping A and B resonances, determination of the peak positions is not as precise as for the case of complex **1a**. Nevertheless, panels a and b in Figure 4 display the frequency-dependent data along with the respective fits to eq 1 for the A and B resonances. Overall, the qualitative trends in the data obtained for complex **1a** and **1b** are very similar. Even the obtained ZFS parameters are quite similar. For complex **1b**, we obtain: $g_z = 2.17(5)$, $D = -0.632(10)$ cm^{-1}, $B_4^0 = -0.00015(3)$ cm^{-1} for species A, and $g_z = 2.17(5)$, $D = -0.44(1)$ cm^{-1}, $B_4^0 = -0.00012(4)$ cm^{-1} for species B. This gives an average value of $D = -0.54$ cm^{-1}, i.e., about 10% less than for complex **1a**. This again agrees reasonably well with reduced magnetization measurements,[14] although the difference is only 5% for the magnetic studies, i.e. $D = -0.58$ cm^{-1} versus -0.61 cm^{-1}. We note that the ratio between the D values obtained for the A and B molecules for both complex **1a** and complex **1b** is the same ($D_A/D_B = 1.4$), which might be expected because of the similarity of the two structures.

Next, we turn to complex **2**. Figure 5 displays temperature dependent spectra obtained at a frequency of 182 GHz, with the external magnetic field again applied approximately parallel to the crystal *c*-axis. Four clusters of resonances are observed, each having the same qualitative appearance, albeit different overall widths and intensities. In similar fashion to complex **1**, these clusters are assigned to different transitions

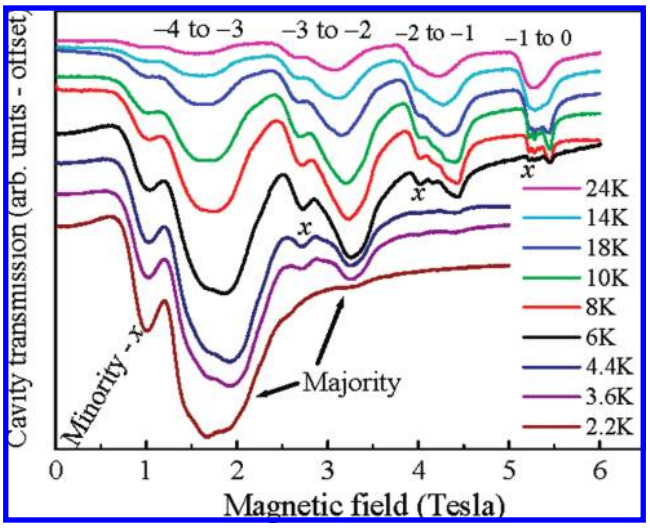

Figure 5. Temperature-dependent spectra for complex **2** at 182 GHz, with the magnetic field applied approximately parallel to the crystal *c*-axis. Four clusters of resonances are observed that each contain an intense major peak and a less intense minor side peak (labeled *x*).

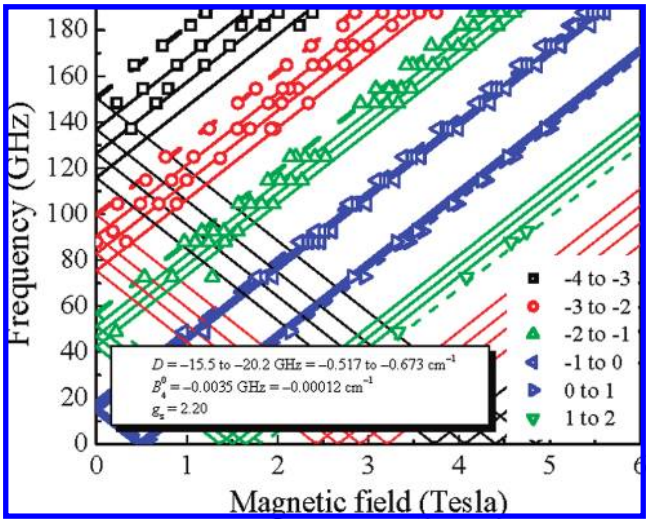

Figure 6. Peak positions obtained from Gaussian fits to data in Figure 5, obtained at 10 K, are plotted as a function of frequency. Superimposed on the data are fits to eq 1 that assume four different *D* values with an $S = 4$ ground state.

within the $S = 4$ multiplet, i.e. the $m_S = -4$ to -3 transitions, etc., as labeled in the figure. Each cluster of resonances contains an intense major peak, and a less intense minor side peak (labeled *x*). Closer examination reveals that each major peak contains several peaks of similar intensity. Indeed, it is possible to obtain reasonably good fits to the data using four Gaussian functions for each cluster of resonances. Thus, it is clear that several distinct molecules exist in crystals of complex **2** also.

The peak positions obtained from Gaussian fits to data such as those in Figure 5 are plotted versus many frequencies in Figure 6. The data points are color and shape coded to distinguish between the different possible transitions within the $S = 4$ state, e.g., the black squares correspond to ground state $m_S = -4$ to -3 transitions, which persist to the lowest temperatures investigated (see Figure 5). One should note that each successive band of resonances is narrower than

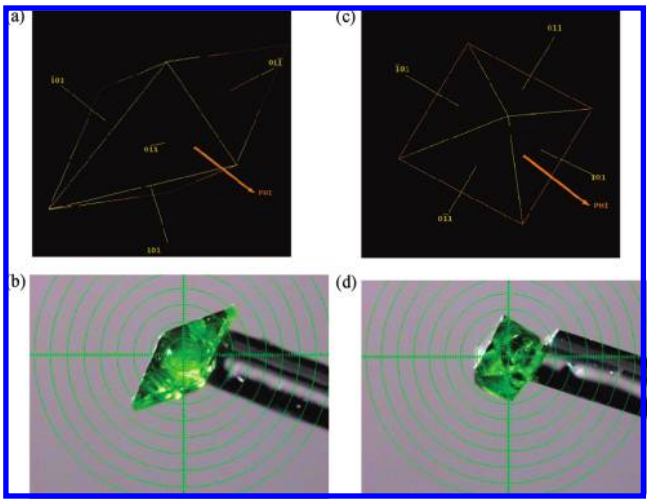

Figure 7. Various faces of a crystal of complex **3**. The crystal has a square bipyramidal shape with the *a* and *b* axes coincident with the two orthogonal edges of the square base, and the *c* axis perpendicular to the *ab* plane. (a) Sketch of the faces of a crystal. (b) Picture of the crystal looking along the *ab* plane. (c) Sketch of the faces of a crystal. (d) Picture of the crystal looking down the *c* axis.

the proceeding one, i.e., the spread in field of the resonances corresponding to different molecular species depends on the m_s values involved in the transition. This type of behavior is indicative of *D*-strain, and has been well-characterized in several other SMMs.[20–22] Superimposed on the data in Figure 6 are fits which assume four different *D* values; the spread in the *D* values is given in the figure, along with the associated *g* and B_4^0 values. As can be seen, all of the data can be explained very well assuming $S = 4$ ground states for all of the molecular species in crystals of complex **2**. The ZFS parameters corresponding to the central majority peaks are: $g_z = 2.20(5)$, $D = -0.610(6)$ cm^{-1}, $B_4^0 = -0.00012(3)$ cm^{-1}. Meanwhile, the ZFS parameters for the minority species (*x* peaks) are: $g_z = 2.20(5)$, $D = -0.670(8)$ cm^{-1}, $B_4^0 = -0.00012(3)$ cm^{-1}. The average *D* value from the majority peaks is very close to the value of $D = -0.60$ cm^{-1} determined by fitting the reduced magnetization versus magnetic field data obtained for a powdered sample of complex **2**.[14]

X-ray data for the EtOH complex again indicate that there are two crystallographically independent molecules in the lattice.[14] There is also a large disorder associated with the ethyl groups on the EtOH ligands. Thus, a reasonable interpretation of the HFEPR spectrum of complex **2** is that the multiplicity of peaks is related to the combined effects of ligand disorder and the occurrence of two crystallographically distinct molecules in the lattice. Indeed, later in this article, we provide direct evidence indicating that weak ligand disorder can cause significant splittings in the EPR spectra of a third Ni_4 complex (**3**). It is important to note that the splitting of the spectra for complex **2** is somewhat

(20) Park, K.; Novotny, M. A.; Dalal, N. S.; Hill, S.; Rikvold, P. A. *Phys. Rev. B* **2002**, *65*, 14426.
(21) Park, K.; Novotny, M. A.; Dalal, N. S.; Hill, S.; Rikvold, P. A. *Phys. Rev. B* **2002**, *66*, 14409.
(22) Hill, S.; Maccagnano, S.; Park, K.; Achey, R. M.; North, J. M.; Dalal, N. S. *Phys. Rev. B* **2002**, *65*, 224410.

less than it is for complex **1a**; the ratios of maximum and minimum D values (A and B peaks) is 1.4 for complex **1a** and 1.3 for complex **2** (or only 1.1 for the splitting between the minority peak and the center of the majority peak). Since both complexes are arranged in the crystals in the same fashion, with two distinct crystallographically independent molecules occupying the body center in one case, and the C-face center in the other case, we can compare the difference of geometry between the molecules at the two different sites. Table 4 in ref [14] provides a comparison between the six metal–ligand bond lengths for complexes **1** and **2** in their two different crystal sites. It can be seen that, except for the metal−chloride bond, the differences for complex **1** are all bigger than those found for complex **2**. Furthermore, there are differences in the bond angles associated with the two crystallographically independent molecular sites in complexes **1** and **2**, with the differences in complex **1** being of greater magnitude than in complex **2**. Therefore, a plausible explanation for the larger field separation of the peaks for complex **1** is that the two crystallographically independent molecules have larger bond length differences and larger angular distortions than those exhibited in complex **2**, and that this leads to larger differences in the ligand fields and, therefore, larger differences in the ZFS parameters for complex **1a** than for complex **2**.

The relatively broad nature of the EPR peaks seen for complexes **1** and **2** can be attributed mainly to distributions in the local environments surrounding individual Ni_4 SMMs.[20–22] It is now well-documented that disorder associated even with weakly (hydrogen) bonding solvate molecules can cause significant distributions in the g-, D-, and E-values for SMMs such as Mn_{12}-acetate.[8–13,23] Such strains have a pronounced effect on HFEPR line widths and shapes.[22,23] Indeed, HFEPR measurements provide the most direct means for characterizing such distributions, which can ultimately have a profound influence on the low-temperature quantum dynamics of the highest symmetry SMMs such as Mn_{12}-acetate.[9,13] Both complexes **1** and **2** contain H_2O solvate molecules in their lattices. We shall see in the following section that the removal of H_2O solvate molecules from the structure results in dramatically sharper EPR spectra. Thus, we suspect that the EPR spectra of complexes **1** and **2** are first split into two series of resonances (A and B peaks) corresponding to the molecules at the body-center and C-face center of the unit cell. These EPR peaks are then further split/modulated due to the effects of ligand disorder. Finally, molecule-to-molecule variations in the hydrogen bonding environments formed by disordered water solvate molecules represent the main source of broadening of the individual EPR peaks resulting from the A and B sites and associated ligand disorder.

We end this section by considering the effects of inter-SMM exchange interactions, which are known to be significant for complexes **1** and **2**. In fact, an antiferromagnetic exchange bias has been observed in the low-temperature hysteresis loops for all three complexes (**1a**, **1b**, and **2**)[14] which is of a similar magnitude to the well-characterized $S = 9/2$ $[Mn_4]_2$ dimer system.[24,25] The major difference between the Mn_4 dimer and the Ni_4 systems is the fact that the intermolecular exchange interaction is confined to a pair of SMMs in the former case, which means that the dimer Hamiltonian is amenable to matrix diagonalization [matrix dimension is $(2S + 1) \times (2S + 1) = 100$], i.e., exact solution. Unfortunately, such an approach is not possible for the Ni_4 complexes **1a**, **1b**, and **2**, for which each Ni_4 unit interacts with many near neighbors. However, one can speculate as to the effects of 3D intermolecular exchange interactions on the HFEPR spectra. As seen for the case of the dimer, the multiplicity of the spectrum increases dramatically, with new EPR peaks emerging from the unperturbed peaks.[25] However, much of the EPR intensity remains centered at the locations of the unperturbed peaks, particularly for $J/D < 0.1$. In fact, the position of the ground-state transition of the dimer $[(-{}^9/_2,-{}^9/_2) \rightarrow (-{}^9/_2,-{}^7/_2)_S]$ is completely unaffected by the exchange (see Figure 1 of ref 25). Thus, it is reasonable to assume that the same will be true for multi-SMM interactions. It is only possible to observe the effects caused by the intradimer exchange interactions in the $[Mn_4]_2$ complex because the intrinsic EPR linewidths are small. Indeed, many of the exchange-induced splittings are barely resolvable. In contrast, we believe that the effects of intermolecular exchange interactions are buried within the inhomogeneous linewidths for the Ni_4 complexes **1a**, **1b**, and **2**. Indeed, the inhomogeneous linewidths for comparable transitions differ by about a factor of 5 between the $[Mn_4]_2$ dimer system and the present complexes (the S and D values are quite comparable); this factor does not take into account the A and B splitting, which is obviously much greater than the inhomogeneous line width. Consequently, the obtained EPR spectra presented in this section *do not* conflict with the findings of magnetic hysteresis measurements,[14,26] i.e. that there exist significant intermolecular interactions in complexes **1a**, **1b**, and **2**. Nevertheless, it is likely that exchange interactions will provide an additional contribution to the line widths/shapes, i.e., exchange probably also contributes to the broad lines and some of the temperature-dependent shifts. However, given the disorder in these systems, it likely represents a challenge to separate the various contributions to the EPR line widths. We note, however, that it could be possible to apply approximate methods to gain further insights into the effects of intermolecular exchange,[27] though such an undertaking is beyond the scope of this investigation. In the following section, we present HFEPR data for a fourth Ni_4 complex (**3**) where the effects of intermolecular interactions can be clearly seen due to the fact that this complex exhibits much sharper EPR spectra. One final point that is

(23) Takahashi, S.; Edwards, R. S.; North, J. M.; Hill, S.; Dalal, N. S. *Phys. Rev. B* **2004**, *70*, 094429.

(24) Hill, S.; Edwards, R. S.; Aliaga-Alcalde, N.; Christou, G. *Science* **2003**, *302*, 1015.

(25) Hill, S.; Wilson, A. *J. Low Temp. Phys.* **2006**, *142*, 267.

(26) Yang, E.-C.; Wernsdorfer, W.; Hill, S.; Edwards, R. S.; Nakano, M.; Maccagnano, S.; Zakharov, L. N.; Rheingold, A. L.; Christou, G.; Hendrickson, D. N. *Polyhedron* **2003**, *22*, 1727–1733.

(27) Gahan, B.; Mabbs, F. E. *J. Chem. Soc., Dalton Trans.* **1983**, *1983*, 1695.

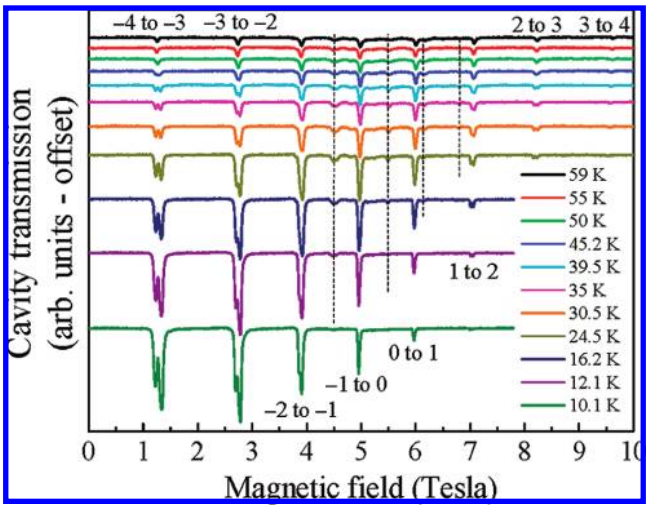

Figure 8. Easy axis HFEPR data for a single crystal of complex **3** at 172 GHz. The spectra exhibit flat base lines and sharp EPR peaks and all 8 transitions within the $S = 4$ state are observed. Peaks that have been highlighted with vertical dashed lines correspond to transitions between states in higher lying ($S < 4$) multiplets.

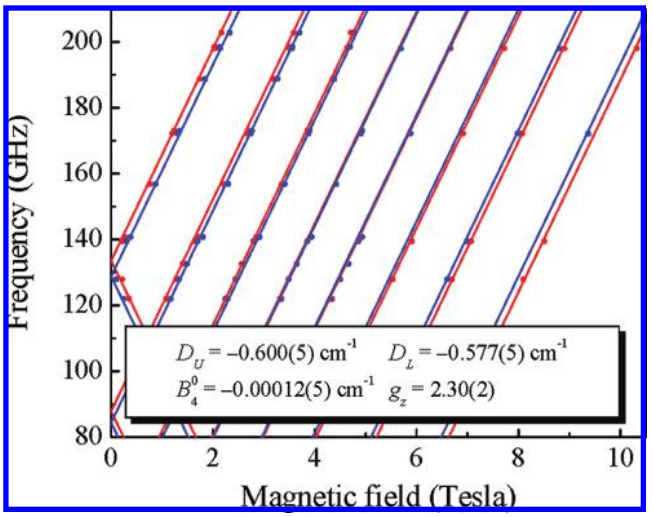

Figure 9. Plot of the positions of the two distinct Ni_4 species for complex **3** obtained at 10 K, as a function of the measurement frequency. The data have been fit to eq 1 with an $S = 4$ ground state.

worth noting is the deviation between the experimental data and the fits for complex **1b** (Figure 4) for the smaller $|m_S|$ transitions, e.g., $m_S = -1$ to 0. A similar shift of the resonances to higher fields, as compared to the single-molecule calculations, is seen for the smaller $|m_S|$ transitions in the $[Mn_4]_2$ dimer.[24,25] Therefore, we speculate that the poor quality of the fit for complex **1b** could be a manifestation of intermolecular exchange interactions, which are believed to be the strongest for this complex.

HFEPR for [Ni(hmp)(dmb)Cl]$_4$, Complex 3. There are several reasons why complex **3** gives the most revealing HFEPR spectra. First of all, the crystal structure of this complex is different than that of the MeOH and EtOH complexes **1a**, **1b**, and **2**; in the case of complex **3**, there is only one crystallographically distinct Ni_4 molecule.[14] This structural difference reflects in part, the steric bulk of the 3,3′-dimethyl-1-butanol (dmb) ligand. Second, not only are there no H_2O solvate molecules in the crystal, but in fact there are no solvate molecules at all in the crystal of complex **3**. Third, the large aliphatic substituent on the dmb ligand provides good electronic insulation between Ni_4 molecules. Thus, complex **3** does not exhibit a measurable exchange bias in its hysteresis plot of magnetization versus magnetic field.[14,26] Furthermore, the faces of a crystal of complex **3** bear a simple relationship to the unit cell of the complex, as shown in Figure 7, which gives two different views of a typical crystal. As can be seen, the crystal has a square bipyramidal shape with the *a* and *b* axes coincident with the two orthogonal edges of the square base, and the *c* axis perpendicular to the *ab*-plane. This simplifies the determination of the crystallographic directions, and facilitates precise orientation of a single-crystal for angle-dependent HFEPR measurements.

172.2 GHz HFEPR spectra are displayed in Figure 8 for various temperatures in the range from 10 to 59 K, and with the magnetic field aligned with the *c*-axis of a crystal of complex **3**. From the temperature dependence, it is clear that the more-or-less evenly spaced dominant peaks correspond to transitions within the $S = 4$ ground state (see also Figure 9); the weaker peaks (marked by vertical dashed lines) in between the strongest resonances are due to transitions within excited states. As labeled in Figures 8 and 9, all eight transitions within the $S = 4$ state are observed. In comparison to complexes **1a**, **1b**, and **2**, the spectra exhibit flat base lines and sharp EPR peaks. This may be due in part to the bulky aliphatic groups that minimize intermolecular interactions. However, the more likely reason is the absence of solvate molecules, thus resulting in a reduced distribution of microenvironments. Nevertheless, a striking feature of the spectra is the splitting of several of the peaks, particularly for transitions involving states with larger absolute m_S values (at low and high fields). This m_S dependence again implies at least two distinct Ni_4 species, with slightly different *D* values, even though high-temperature X-ray data suggest otherwise. Indeed, frequency dependent studies confirm this conclusion, as shown in Figure 9, where all of the $S = 4$ peak positions have been fit to eq 1 assuming the same *S*, *g*, and B_4^0 values, and two slightly different *D* values (red and blue lines). The obtained parameters are: $g_z = 2.3$, $D = -0.60$ cm^{-1}, and $B_4^0 = -0.00012$ cm^{-1} for the higher frequency peaks; and $g_z = 2.3$, $D = -0.58$ cm^{-1}, and $B_4^0 = -0.00012$ cm^{-1} for the lower frequency peaks. Again,the *D* values from HFEPR measurements are quite close to those obtained from fitting the reduced magnetization data,[14] which gives a value of $D = -0.61$ cm^{-1}. The actual linewidths of the fine structures in Figure 8, and the m_S dependence of these widths, is markedly less than for complexes **1** and **2**; the ratio of the linewidths of the $m_S = -4$ to -3 and m_S -1 to 0 transitions is 2 for complex **3**, and about 4 for complexes **1** and **2**. This is indicative of weaker *D*-strain associated with each of the lattice sites in complex **3**, which again hints at the dramatic effect the solvent of crystallization can have on the distributions of microenvironments and resulting ZFS parameters.

The fact that the fits in Figure 9 agree so well with the m_S dependence of the peak splitting provides compelling support for the existence of two distinct Ni_4 species. A closer

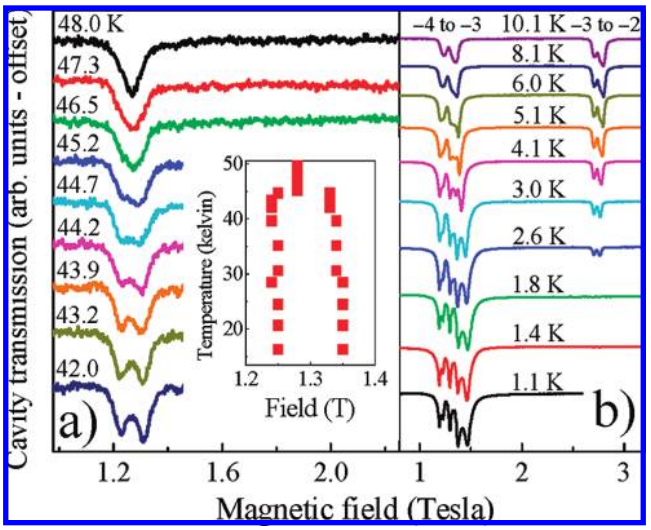

Figure 10. (a) Plot of 172 GHz temperature dependence at close temperature intervals. The inset shows the peak splitting appears very abruptly below a critical temperature of about 46 K, suggesting a possible structural transition. (b) Additional broadening and splitting of the EPR spectra is observed at temperatures below about 6 K.

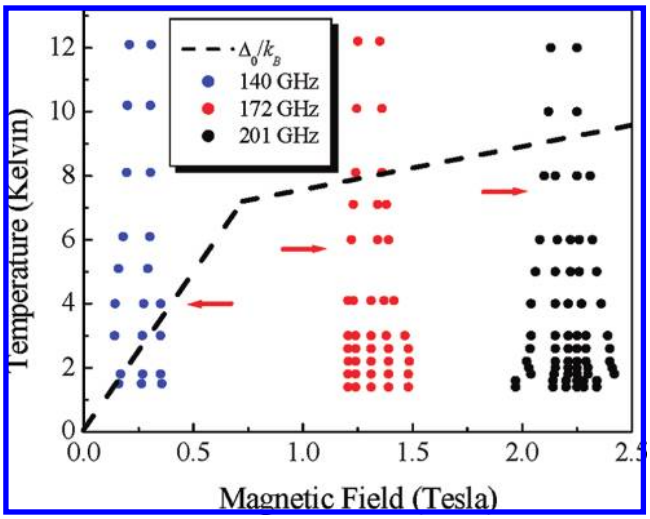

Figure 11. Plot of the positions of peak splittings at low temperatures for three frequencies. The dashed line represents the energy separation, Δ_0/k_B, between the $m_S = -4$ ground-state and the first excited state ($m_S = +4$ for $B < 0.66$ T, and $m_S = -3$ for $B > 0.66$ T). The red arrows give an indication at which temperature additional splittings appear for a given frequency.

examination of the 172 GHz EPR spectra (Figure 10a) indicates that the splitting is absent above about 46 K. In fact, measurements performed at closely spaced temperature intervals reveal that the splitting appears very abruptly below a critical temperature of about 46 K, as shown in the inset to Figure 10a. This suggests a possible structural transition at 46 K, which could lead to a lowering of the crystallographic symmetry and, hence, to distinct Ni_4 species, as was the case for complexes **1a**, **1b**, and **2**. This scenario is supported by thermodynamic studies and low-temperature X-ray measurements presented at the end of the article, which suggest that the two fine structure peaks may be explained in terms of a weak static disorder associated with the dmb ligand which sets in below 46 K.

Upon cooling complex **3** to ~1 K, additional broadening and splittings of the EPR spectra are observed at temperatures below about 6 K, as shown in Figures 10b and 11. At least four (possibly up to six) ground-state fine structure peaks are seen at the lowest temperatures between ~1.15 and 1.5 T in Figure 10b. It is very clear that these fine structure splittings cannot be attributed to (static) structurally different microenvironments, as we now outline. First of all, if this was the source of the splitting, then it should be apparent for all transitions, including the $m_S = -3$ to -2 resonance, which is observed down to 2.6 K at around 2.7 T in Figure 10b. However, there is no broadening and only two fine structure peaks are observed for this resonance to temperatures well below 6 K, which is where the additional fine structures begin to emerge in the ground-state resonance. Studies to higher frequencies (Figure 11) indicate that the fine structures in the ground-state resonance ($m_S = -4$ to -3) persist to the same field range (~2.5 T) where the $m_S = -3$ to -2 resonance is seen in Figure 10b. Consequently, one can rule out field-dependent structural changes. In fact, as seen in Figure 11, the temperature below which the additional fine structures begin to appear increases with increasing magnetic field/frequency (see red arrows in Figure 11 as rough guide). For comparison, the dashed line in Figure 11 represents the energy separation, Δ_0/k_B, between the $m_S = -4$ ground-state and the first excited state ($m_S = +4$ for $B < 0.66$ T, and $m_S = -3$ for $B > 0.66$ T). Thus, it appears as though the onset of the additional fine structures is related to the depopulation of excited states. Indeed, similar evidence for diverging linewidths has been reported previously for this same temperature regime,[22] i.e., when $k_BT < \Delta_0$. However, these earlier studies involved SMMs with broad EPR lines compared to the present Ni_4 complex **3**, making it difficult to clearly resolve additional EPR fine structures brought on by intermolecular exchange interactions. For this reason, studies of the present Ni_4 complex (**3**) provide an excellent opportunity to better understand the effects of intermolecular exchange on the EPR spectra of SMMs.

Although most aspects of earlier EPR line width studies on $Mn_{12}Ac$ and Fe_8 have been understood in terms of competing exchange and dipolar interactions,[20–22] an explanation for the behavior of the ground-state resonance ($m_S = -4$ to -3 in the present study) has remained elusive for $k_BT < \Delta_0$. We speculate that this behavior is related to the development of short-range intermolecular magnetic correlations/coherences (either ferro- or antiferromagnetic) which are exchange averaged at higher temperatures. In principle, this should result simply in a shift of the EPR spectrum. However, since this phenomenon involves the interaction between multiple molecules, of which there are two inequivalent types (the two fine structure peaks observed from 10 to 46 K), one anticipates an increase in the number of fine structure peaks corresponding to the development of short-range correlations between different combinations of the two molecular species having slightly different D values. In addition, the very fact that there clearly exist different molecular species also suggests that there may be differences in the interaction strengths between various pairs of molecules.

Additional evidence for short-range magnetic exchange interactions in complex **3** comes from single-crystal HFEPR studies of the single Ni^{II} ions in a $[Zn_3Ni(hmp)_4(dmb)_4Cl_4]$ complex doped into a crystal of the isostructural diamagnetic $[Zn(hmp)(dmb)Cl]_4$ complex.[28] In these studies, the doping level was chosen so that the compound contained a small fraction of magnetic molecules which are well isolated from one another by the nonmagnetic $[Zn(hmp)(dmb)Cl]_4$ molecules. Interestingly, the Zn analog of complex **3** shows a similar structural transition just below 50 K (see below). However, similar temperature dependent HFEPR studies on this compound revealed no extra splittings of the ground-state EPR peaks at low temperatures. Thus, we speculate that this null result is due to the isolation of the magnetic species in the doped diamagnetic lattice, i.e., there exists no possibility for short-range (nearest neighbor) intermolecular interaction. Without such a possibility, no extra peak splittings appear.

Without a more detailed understanding of the disorder, and of the nature of the intermolecular interactions, it is not possible to give a more precise explanation for the low temperature spectrum of complex **3**. Nevertheless, the observation of 3D ordering in this compound does signify the relevance of intermolecular interactions, either because of dipolar interactions or weak superexchange. One can expect short-range magnetic correlations to develop well above the long-range thermodynamic ordering temperature and, therefore, that it is these shorter range correlations that impact the EPR spectrum in terms of additional fine-structure splittings.

Microenvironments, Phase Transition, and Heat Capacity Measurements for Complex 3. To ascertain the origin of the fine structure splitting observed in the HFEPR spectra below 46 K (Figure 10a), we carried out detailed heat capacity measurements in the temperature range from 2 to 100 K. The results are given in Figure 12a, where it can be seen from the plot of heat capacity at constant pressure (C_P) versus temperature that there is a peak at 46.6 K (blue data in Figure 12a) which corresponds very well to the temperature at which the peaks in the HFEPR spectrum start to split (Figure 10a). Heat capacity measurements were also performed for a Zn analog of complex **3** (containing trace amounts of Ni, ~2.5%) in order to determine whether the phase transition observed at 46.6 K is due to a structural change that causes different microenvironments, or whether it perhaps arises from a spin related phenomenon such as magnetic ordering due to intermolecular magnetic exchange interactions. The diamagnetic Zn analog, which has the same structure as complex **3**, also exhibits a heat capacity peak at an almost identical temperature (49.6 K, red data in Figure 12a), suggesting that it cannot be the result of a magnetic phase transition. The fact that the two structurally analogous complexes have this peak with similar amplitude at about the same temperature indicates that it is due to a structural

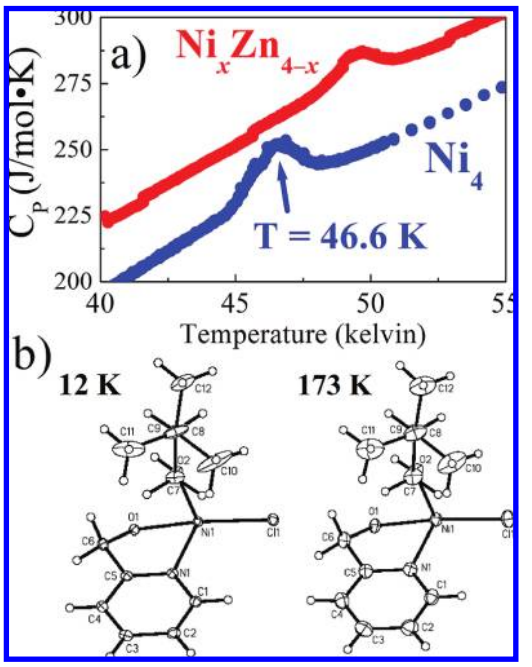

Figure 12. (a) Plot of heat capacity at constant pressure (C_P) versus temperature for complex **3** (blue data) and the Ni doped Zn analog,[28] which has the same structure as complex **3** (red data). (b) The thermal ellipsoid plot comparison of symmetry independent parts of the molecule of complex **3** at 12 and 173 K.

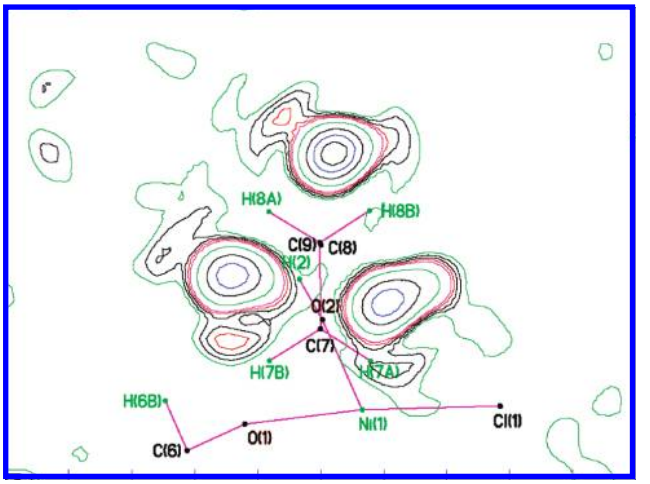

Figure 13. Difference electron density of the three methyl groups for complex **3** at 12 K.

phase transition, perhaps associated with the ligand.

To determine the entropy involved in the phase transition, we first subtracted a baseline contribution from the data. The choice of an appropriate baseline correction in this temperature regime can be somewhat difficult. Neglecting the transitions themselves, we approximated the data between 40 and 60 K as a straight line. The entropy obtained through the resulting "excess" heat capacity was then determined by the standard thermodynamic relationship

$$\Delta S = \int \frac{C_P(T)}{T} d\mathrm{T} \qquad (2)$$

The entropy gained in the phase transition is about 1.9 J/mol·K, corresponding to $\Delta S = R \ln(1.3)$ in comparison to the $R \ln(3)$ expected for the three methyl sites. This relatively

(28) Yang, E.-C.; Kirman, C.; Lawrence, J.; Zakharov, L. N.; Rheingold, A. L.; Hill, S.; Hendrickson, D. N. *Inorg. Chem.* **2006**, *44*, 3827–3836.

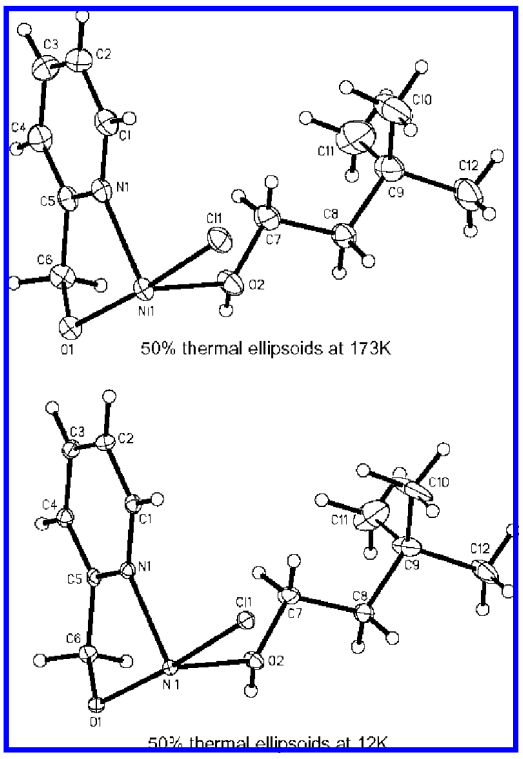

Figure 14. Structural comparison of complex **3** between 173 and 12 K (50% probability level thermal ellipsoids).

small value for ΔS might involve motion left over from tunneling of the dmb methyl hydrogen atoms.

Low-Temperature X-ray Structure of Complex 3. To further confirm that the 46 K peak splitting observed in the HFEPR spectra stems from different microenvironments, we collected single-crystal X-ray diffraction data for complex **3** at a temperature of 12(2) K. The thermal ellipsoid plot comparison of symmetry independent parts of the molecule at 12 and 173 K are given in Figure 12b. Interesting thermal ellipsoids in the t-butyl group from 3,3-dimethyl-1-butanol are evident in both plots. This should be where the order–disorder activity is taking place. The most remarkable thing is that the thermal ellipsoids shrink at 12 K for all the atoms except for the t-butyl group. These abnormal looking ellipsoids are indeed much larger than would be expected. Yet, the positions of the methyl group do not seem to be split. The electron density in a difference map for the three methyl groups was computed and is shown in Figure 13. If the methyl groups were rotating around the C8−C9 bond, they would start to look more peanut-like or other regions of density would show up. Instead, they mirror the anisotropic behavior of the thermal ellipsoid plot (this is the same orientation as the bottom of Figure 14). Also, the thermal ellipsoid in Figure 13 implies that the motion is a clockwise rocking around the O2−C7 bond. Indeed, it is shown in Figure 15 that a very slight clockwise shift of the structure

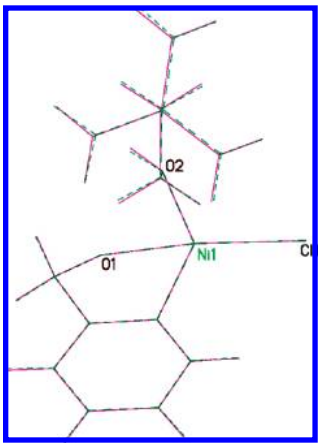

Figure 15. Structural comparison of complex **3** between 173 and 12 K.

obtained at 12 K mapped onto the 173 K structure. This small change in the structure supports the suggestion that different microenvironments cause the HFEPR peak splitting at low temperature.

Conclusion

HFEPR data have been collected for four different Ni_4 SMMs. The spin ground state ($S = 4$) and axial ZFS parameters were deduced on the basis of easy-axis spectra collected at many different microwave frequencies. Complexes **1a**, **1b**, and **2** exhibit broad and unusually shaped peaks, as well as multiple ground-state transitions, indicating a large amount of disorder in these systems. The multiplicity of the ground-state resonance stems partly from the fact that there exist two crystallographically independent molecules in the lattices of complexes **1a**, **1b**, and **2**. Nevertheless, disorder also plays an important role in the lineshapes also. This disorder appears to involve both the ligands and the H_2O solvate molecules in the structure. In contrast, crystals of complex **3** contain no H_2O solvate molecules. Consequently, the EPR spectra exhibit very sharp, narrow resonances. However, a structural transition involving the $HOCH_2CH_2C(CH_3)_3$ ligand that occurs below 46 K gives rise to two species of molecules in the crystal, evident from peak splittings. At temperatures below 6 K additional splittings of the ground-state transition are seen due to intermolecular exchange interactions. The ability to resolve these intermolecular interactions, which are present in all complexes, is attributed to the high quality and narrow EPR linewidths associated with complex **3**. These findings once again highlight the dramatic influence of the solvate molecules on the quantum properties of SMMs.

Acknowledgment. This work was supported by the National Science Foundation (DMR0506946, DMR0239481, and CHE0350615).

IC701416W